A theoretical study of the low-lying excited states of thieno[3,4-*b*]pyrazine

María D. Gómez-Jiménez, Rosendo Pou-Amérigo, and Enrique Ortí[a)]
Instituto de Ciencia Molecular, Universidad de Valencia, P.O. Box 22085, Valencia 46071, Spain

(Received 3 September 2009; accepted 24 November 2009; published online 28 December 2009)

The low-lying electronic excited states of thieno[3,4-*b*]pyrazine have been studied using the multiconfigurational second-order perturbation CASPT2 theory with extended atomic natural orbital basis sets. The CASPT2 results allow for a full interpretation of the electronic absorption and emission spectra and provide valuable information for the rationalization of the experimental data. The nature, position, and intensity of the spectral bands have been analyzed in detail. A preliminary comparative study of the ground-state geometry of thieno[3,4-*b*]pyrazine has been performed at the coupled cluster single and doubles and density functional theory levels using a variety of correlation-consistent basis sets. Thieno[3,4-*b*]pyrazine exhibits a polyene-like structure in the ground state due to the bond localization in the pyrazine moiety. An aromatization of the pyrazine unit is predicted for the lowest-energy electronic excited states. © *2009 American Institute of Physics*. [doi:10.1063/1.3274816]

I. INTRODUCTION

The development of low-bandgap polymers has been the subject of much interest in recent years motivated by their technologically attractive physical properties, their intrinsic electrical conductivity, their interesting optical properties, and their amphoteric electrochemical behavior.[1] The synthesis of poly(isothianaphthene) (pITN),[2] whose bandgap (E_g = 1.1 eV) is about 1 eV lower than that of the parent polythiophene, showed up the possibility of tuning the polymer bandgap by modifying the structure of the conjugated backbone. pITN was designed on the basis of the idea that fusion of a benzene ring to the thiophene ring would promote the quinoidal character of the polythiophene chain, thereby reducing the bandgap. Since then, much effort has been devoted, both theoretically and experimentally, to explore the relationship between the chemical structure of conjugated polymers and their bandgap in order to further reduce the size of the latter.[1]

Thieno[3,4-*b*]pyrazine (TP), for which the benzene ring of ITN is replaced by a pyrazine ring (see Fig. 1), has been shown to be an excellent precursor for the production of low-bandgap conjugated oligomers and polymers. The presence of nitrogen atoms improves the processability of the polymer and reduces the steric interactions between adjacent monomeric units that force the pITN polymer to adopt a nonplanar conformation.[3,4] The interest in TP conjugated derivatives began in 1990 when theoretical calculations predicting a very small bandgap (0.70 eV) for polyTP (pTP) were reported.[5,6] After this prediction, general synthetic routes have been developed to obtain different derivatives of pTP. Pomerantz and co-workers[7] prepared poly(2,3-dihexylTP) for which a bandgap of 0.95 eV was estimated. More recently, Rasmussen *et al.*[8] investigated the electropolymerization of various 2,3-disubstituted TPs and obtained bandgap values of only 0.66–0.79 eV, which lie in the range predicted theoretically for nonsubstituted polyTP. From these preliminary studies, TP has been used as a building block to modulate the bandgap when mixed with other heterocyclic units in conjugated oligomers and polymers.[9] This strategy has given rise to a wide range of applications such as transparent conductors, light-emitting materials,[10] thin film transistors,[11] photovoltaic devices,[12] solar cells,[13] and polymeric electrochromics for data storage.[14]

To fully understand the electronic and optical properties of the conjugated systems derived from TP, it is necessary to have an in-depth knowledge of the structure and properties of the monomeric precursor. In this sense, the characterization of TPs is rather limited. The first reports on TP were the synthesis of the 2,3-diphenyl- and 2,3-dimethyl-derivatives in 1957[15] and 1981,[16] respectively, but it was not until 2002 that the first full characterization of TPs was reported.[17] In this and later studies, Rasmussen included the X-ray geometry determination of 2,3-dimethyl-TP and the photophysical characterization of a series of monomeric 2,3-difunctionalized TPs including the nonsubstituted TP.[17–19] The structure and the absorption spectra of TP were theoretically calculated using semiempirical methods.[19] The semiempirical results provided a qualitative description of the low-energy region of the spectrum, the interpretation of the high-energy bands being rather limited.

In the present contribution, a detailed theoretical study of the structural and electronic properties of TP has been carried out. Density functional theory (DFT), coupled cluster (CC), and multiconfigurational second-order perturbation theory methodologies have been employed in order to analyze the geometrical structure and to elucidate the nature, position, and intensity of the bands of the absorption and emission spectra. Since the theoretical study of more extended systems such as oligomers and polymers is of high interest to develop low-bandgap materials, we will addition-

[a)]Electronic mail: enrique.orti@uv.es.

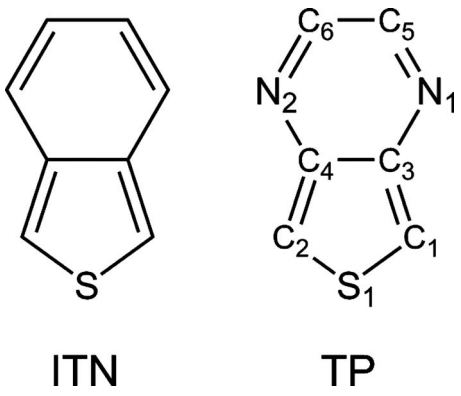

FIG. 1. Chemical structure of ITN and TP. Atom numbering is given for TP.

ally check whether the DFT approach can be a valuable alternative to more expensive computational methods for this kind of systems.

II. COMPUTATIONAL DETAILS

The ground-state geometry of TP was optimized by using the DFT approach and the coupled cluster singles and doubles (CCSD) method.[20] For the DFT calculations, the Becke's three-parameter B3LYP exchange-correlation functional was employed.[21,22] The correlation-consistent cc-pVDZ, cc-pVTZ, and aug-cc-pVDZ basis sets[23] were utilized for geometry optimizations.

For the computation of the vertical excitation energies, the complete-active-space self-consistent-field (CASSCF) approximation was used in combination with a multiconfigurational second-order perturbation approach, the CASPT2 method.[24,25] CASSCF/CASPT2 calculations reproduce vertical excitations energies of organic molecules usually within 0.2 eV.[26] The active space includes the π and π^* valence molecular orbitals (9 MOs), two σ orbitals which correspond to the lone pairs of nitrogen atoms, and 14 electrons (10π and 4σ electrons). CASSCF/CASPT2 calculations were performed making use of atomic natural orbital (ANO) type basis sets contracted with the schemes: [3s2p1d] for carbon and nitrogen atoms, [4s3p1d] for sulfur, and [2s] for hydrogen.[27]

The basis set was supplemented with a set of specifically designed 1s1p1d rydberg-type functions, contracted from a set of 8s8p8d primitives, placed in the averaged charge centroid of the $^2A_2$, $^2B_1$, and $^2A_1$ states of the cation.[28] Such an enlargement of the basis set is required for the adequate representation of the rydberg excited states. Thus, apart from valence states, the lowest members of the rydberg series converging to the first ionization potential have also been taken into account for the neutral system, extending the active space to include the 3s, 3p, and 3d orbitals. The simultaneous inclusion of nine one-electron functions would yield an excessive number of active orbitals. Thus, the enlargement was carried out by adding selected sets of rydberg orbitals to the valence space. To avoid singularities, an imaginary shift of 0.2 a.u., selected through calibration, was introduced.[29] The CASSCF state-interaction (CASSI) method was employed to compute the oscillator strength.[30,31] Energy differences corrected by CASPT2 correlation energies were used in the oscillator strength formula. Solvent effects were considered within the self-consistent reaction field theory using the polarized continuum model (PCM) approach to model the interaction with the solvent.[32] The PCM model considers the solvent as a continuous medium with a dielectric constant ε, and represents the solute by means of a cavity built with a number of interlaced spheres.[33]

DFT and CCSD calculations were carried out making use of the C.02 revision of the GAUSSIAN03 suite of programs.[34] CASSCF/CASPT2 calculations were performed with the MOLCAS-6.4 program package.[35]

III. RESULTS AND DISCUSSION

A. Ground-state geometry

TP is predicted to have a planar conformation (C_{2v} symmetry) in its ground electronic state ($1\ ^1A_1$). Table I collects the bond distances and bond angles optimized at the DFT and CCSD levels using the cc-pVDZ, cc-pVTZ, and aug-cc-pVDZ basis sets. Theoretical data are compared with averaged X-ray data obtained from the experimental structures reported by Rasmussen *et al.* for 2,3-dimethyl-TP,[17] 2,3-dihexyl-TP,[36] and 2,3-bis(bromomethyl)-TP.[37] Table I further includes the computed and microwave geometries[38] of the thiophene molecule for comparison purposes. The atom numbering used in this section corresponds to that depicted in Fig. 1 for TP.

As shown by the bond distances summarized in Table I, the TP molecule, in its ground state, exhibits a pro-quinoid structure. The fusion of the pyrazine ring with the parent thiophene ring involves the lost of the aromaticity in the pyrazine unit, whereas the geometry of thiophene remains almost unaltered. At the CCSD/cc-pVTZ level, the C_3-N_1 and C_4-N_2 bonds have a length of about 1.380 Å, while the N_1-C_5 and N_2-C_6 bonds are much shorter and have a length of 1.296 Å. These bond distances are drastically different from those calculated at the CCSD/cc-pVTZ level for the pyrazine ring (1.333 Å). TP therefore shows a 3,6-diaza-octatetraene-type structure with a marked single-double bond length alternation (BLA) along its periphery and should be better visualized as resulting from the linkage of a diazadiene unit to the thiophene ring. The single-double alternation can be quantified taking $\Delta R_{C-C}=R(C_5-C_6)-R(C_1-C_3)$ and $\Delta R_{N-C}=R(C_3-N_1)-R(N_1-C_5)$ as measures of the BLA of C–C and N–C bonds, respectively. At the CCSD/cc-pVTZ level, ΔR_{C-C} and ΔR_{N-C} take values of 0.075 and 0.085 Å, respectively, showing the polyene-like structure of TP.

The comparison of the CCSD parameters obtained with the three basis sets shows that the cc-pVDZ and aug-cc-pVDZ basis sets provide almost identical values for the bond lengths and the bond angles of TP. The inclusion of diffuse functions therefore has a negligible effect on the computed geometry. In contrast, the triple-zeta cc-pVTZ basis set leads to a reduction of all bond distances ($\sim$0.01 Å) and especially affects the C–S bonds that shorten by ca. 0.02 Å. The cc-pVTZ basis set indeed provides the best agreement between the computed values and the averaged X-ray data collected in Table I for substituted 2,3-alkyl-TPs.[17,36,37] The comparison between CCSD/cc-pVTZ results and X-ray data

TABLE I. Experimental and computed geometries for the ground state of TP and thiophene (bond distances in angstroms and angles in degrees).

	Thieno[3,4-*b*]pyrazine							Thiophene						
	CCSD			B3LYP			Expt.[a]	CCSD			B3LYP			Expt.[b]
Parameters	cc-pVDZ	cc-pVTZ	aug-cc-pVDZ	cc-pVDZ	cc-pVTZ	aug-cc-pVDZ		cc-pVDZ	cc-pVTZ	aug-cc-pVDZ	cc-pVDZ	cc-pVTZ	aug-cc-VDZ	
S_1-C_1	1.725	1.707	1.728	1.722	1.708	1.722	1.692	1.740	1.725	1.743	1.738	1.727	1.739	1.714
C_1-C_3	1.388	1.376	1.389	1.387	1.380	1.387	1.371	1.376	1.362	1.378	1.371	1.363	1.372	1.370
C_3-C_4	1.448	1.436	1.450	1.453	1.446	1.453	1.432	1.443	1.430	1.443	1.431	1.423	1.431	1.423
C_3-N_1	1.393	1.380	1.393	1.373	1.366	1.372	1.374							
N_1-C_5	1.308	1.296	1.309	1.311	1.303	1.309	1.305							
C_5-C_6	1.464	1.451	1.467	1.443	1.435	1.443	1.464							
$C_1-S_1-C_2$	93.39	93.86	93.57	93.90	94.25	94.00	93.86	91.35	91.54	91.41	91.49	91.64	91.50	92.17
$S_1-C_1-C_3$	110.81	110.49	110.59	110.49	110.34	110.38	110.97	111.96	111.76	111.86	111.53	111.45	111.51	111.47
$C_1-C_3-C_4$	112.50	112.59	112.63	112.56	112.53	112.62	111.93	112.36	112.47	112.44	112.72	112.73	112.74	112.45
$C_4-C_3-N_1$	122.31	121.97	122.08	121.81	121.50	121.60	121.53							
$C_3-N_1-C_5$	113.43	114.10	113.94	114.42	115.00	114.85	115.98							
$N_1-C_5-C_6$	124.27	123.94	123.98	123.78	123.50	123.55	122.31							

[a]X-ray data averaged from the structures reported for 2,3-dimethyl-TP (Ref. 17), 2,3-dihexyl-TP (Ref. 36), and 2,3-bis(bromomethyl)-TP (Ref. 37).
[b]Microwave data from Ref. 38.

TABLE II. Vertical excitation energies (ΔE, in eV) and oscillator strengths (f) calculated for the electronic states of TP compared with experimental data.

	CASSCF	CASPT2		Expt.[a]	
State	ΔE	ΔE	f	ΔE	f
$1\ ^1A_1$ [b]					
$1\ ^1B_1(n\pi^*)$	5.40	3.11	0.008		
$1\ ^1B_2(\pi\pi^*)$	5.37	3.35	0.033	3.54	0.053
$2\ ^1A_1(\pi\pi^*)$	5.08	3.82	0.091	3.99–4.15	0.184
$3\ ^1A_1(\pi\pi^*)$	7.06	5.11	0.321	5.41	0.391
$2\ ^1B_2(\pi\pi^*)$	7.23	5.20	0.078		
$2\ ^1B_1(n\pi^*)$	8.52	5.45	0.004		
$4\ ^1A_1(\pi\pi^*)$	6.73	5.52	0.012		
$1\ ^1A_2$(Ryd)	6.31	5.64	0.000		
$3\ ^1B_1(\pi\sigma^*)$	7.09	5.67	0.006		
$3\ ^1B_2(\pi\pi^*)$	8.91	5.86	0.009		
$4\ ^1B_2(\pi\pi^*)$	9.11	6.00	0.079		
$5\ ^1A_1(\pi\pi^*)$	9.16	6.09	0.263		
$4\ ^1B_1(n\pi^*)$	8.95	6.16	0.000		
$2\ ^1A_2$(Ryd)	6.73	6.17	0.000		
$6\ ^1A_1(\pi\pi^*)$	8.65	6.22	0.379	6.23	0.412
$5\ ^1B_2$(Ryd)	6.53	6.23	0.020		
$5\ ^1B_1$(Ryd)	7.79	6.43	0.002		
$7\ ^1A_1$(Ryd)	7.31	6.69	0.001		
$6\ ^1B_2$(Ryd)	7.10	6.75	0.000		

[a]Absorption maxima recorded for TP in CH_3CN at room temperature from Ref. 19.
[b]Ground electronic state.

shows up small average deviations of 0.009 Å for the bond lengths and below 1° for the bond angles. The higher deviations observed for the $C_3-N_1-C_5$ (1.9°) and $N_1-C_5-C_6$ (1.6°) angles are probably due to the presence of alkyl substituents in the experimental structure. The geometry of TP was previously calculated using semiempirical methods.[5,39,40] These methods reproduced the bond localization of the pyrazine moiety quite well but failed in predicting the relative length of the C_3-C_4 and C_5-C_6 bonds.

The analysis of the results obtained using the B3LYP approach reveals that this methodology also gives an adequate description of the geometry of TP. The effects of the basis sets are similar to those found with CCSD, and B3LYP/cc-pVTZ calculations lead to average deviations with respect to experiment (0.014 Å for the bond lengths and 0.6° for the bond angles) of the same order than CCSD. Therefore, both CCSD and B3LYP approaches provide a molecular structure that correlates well with the experimental data.

For the thiophene molecule, the existence of an experimental geometry measured in gas phase (microwave data)[38] allows for a more accurate comparison between theory and experiment. The average deviations between the computed results (cc-pVTZ) and the experimental values are now lower than 0.01 Å for the bond lengths and 0.3° for the bond angles at both the CCSD and B3LYP levels. The deviations between CCSD and DFT values are actually of only 0.003 Å and 0.2°. Therefore, DFT turns out to be a valid alternative to CCSD for geometry optimization.

B. Vertical excited states of TP

Table II collects the vertical excitation energies and oscillator strengths calculated at the CASSCF/CASPT2 levels for the electronic states of TP using the B3LYP/cc-pVTZ-optimized geometry of the ground state. The energy ordering of the states corresponds to that determined with CASPT2. The most important electronic configurations describing the excited states of TP and their weights in the CASSCF wave function are summarized in Fig. 2. The available experimental data, taken from the electronic spectrum of TP recorded in CH_3CN at room temperature,[19] have been also included in Table II for the sake of comparison.

Figure 3 sketches the atomic orbital composition of the three highest occupied molecular orbitals (HOMO, HOMO–1, and HOMO–2) and of the lowest unoccupied molecular orbital (LUMO). The HOMO is of π nature and is more localized over the thiophene ring with no contribution from the sulfur atom (a_2 symmetry). The HOMO–2 and the LUMO are also of π nature but with large contributions from the sulfur atom (b_1 symmetry). The HOMO–1 is of σ nature and mainly corresponds to the nitrogen lone pairs. As sketched in Fig. 2, the HOMO, HOMO–1, and HOMO–2 are very close in energy, in only 0.88 eV (B3LYP/cc-pVTZ level), while the LUMO is well separated from the rest of virtual orbitals (2.36 eV). Therefore three close-in-energy electronic transitions involving the HOMO, HOMO–1, HOMO−2→LUMO excitations have to be expected at low energies.

CASPT2 calculations predict the occurrence of two electronic excited states below 3.5 eV (see Table II). They are the $1\ ^1B_1$ and the $1\ ^1B_2$ states, which are computed to lie 3.11 and 3.35 eV above the ground state, respectively. The transition to the former mainly involves the excitation from the HOMO–1 (nitrogen lone pairs) to the LUMO (π^*) and therefore exhibits an $n\pi^*$ character. The transition to the latter

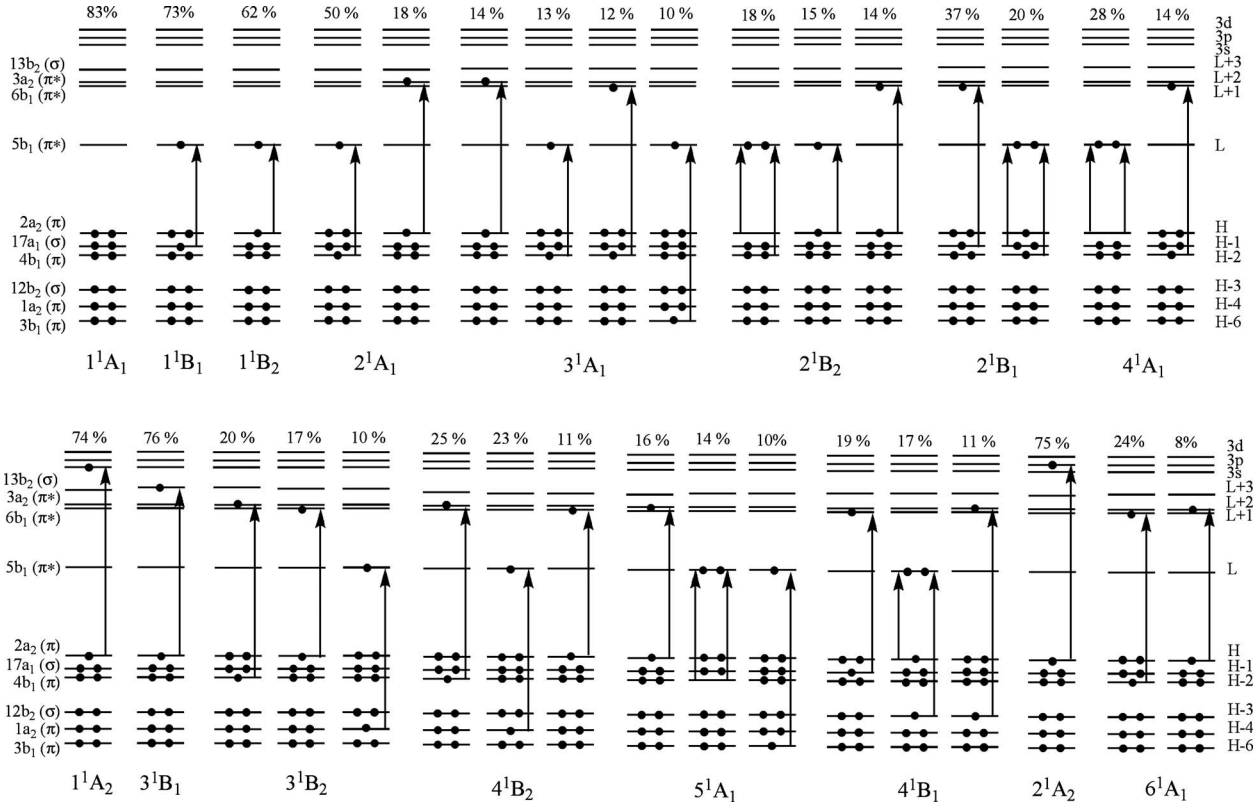

FIG. 2. The most important electronic configurations in the CASSCF wave function for the low-lying states of TP. The orbital occupation and the weight in the wave function are given.

corresponds to a $\pi \rightarrow \pi^*$ excitation from the HOMO to the LUMO. CASPT2 calculations therefore predict the $n \rightarrow \pi^*$ transition to occur at slightly lower energies than the $\pi \rightarrow \pi^*$ transition. Both transitions are computed to be weak and, as expected, the oscillator strength for the $n \rightarrow \pi^*$ excitation is smaller.

The experimental spectrum of TP shows, in this region, a broad and fairly weak band at approximately 350 nm (3.54 eV). In the light of the CASPT2 results obtained here, the transitions to both the $1\ ^1B_1$ and the $1\ ^1B_2$ states are contributing to the feature experimentally observed. Such a conclusion is in accordance with the analysis of analogous compounds performed by Rasmussen *et al.*[19] In this study, it was emphasized that the spectral profile of TP in this region is very similar to that recorded for quinoxaline, which has been attributed to a pyrazine-based $n \rightarrow \pi^*$ transition. However, according to the intensity pattern observed, they concluded that it could be better related to the weakly allowed $\pi \rightarrow \pi^*$ transition observed for isothianaphthene, an isostructural compound, which is located in the same energy region.

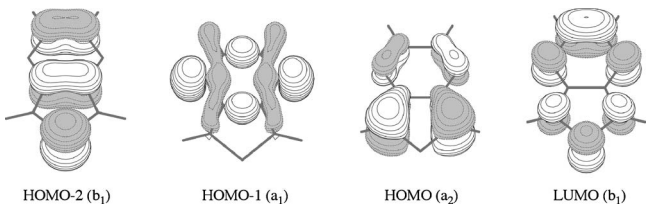

FIG. 3. Electron density contours (0.03 e $Bohr^{-3}$) calculated for selected molecular orbitals of TP at the B3LYP/cc-pVTZ level.

Our calculations support that both transitions are responsible for such an absorption, with the weaker $n \rightarrow \pi^*$ excitation lying under the stronger $\pi \rightarrow \pi^*$ one.

In the region close to 4 eV, the experimental spectrum shows two peaks at 3.99 and 4.15 eV. Due to the close energetic spacing of the bands and their intensity, Rasmussen assigned them to the vibrational structure of only one $\pi \rightarrow \pi^*$ transition.[19] CASPT2 results further support this conclusion. The transition responsible for the two peaks is the excitation to the $2\ ^1A_1$ state calculated at 3.82 eV, which has an oscillator strength of 0.091, three times more intense than the band at 3.35 eV, in agreement with the relative intensities pattern found in the experimental spectrum. The HOMO−2 →LUMO configuration (50%) is mainly involved in this excited state, with a small contribution from the HOMO →LUMO+2 configuration (18%). Our results rule out the existence of any other band contributing to the experimental feature, since no other electronic state is calculated below 5 eV.

At higher-energy regions, an intense band has been detected around 5.41 eV.[19] According to our calculations, it mainly corresponds to the $\pi \rightarrow \pi^*$ transition to the third state of A_1 symmetry, computed at 5.11 eV with a high oscillator strength (0.321). The CASSCF wave function of this excited state exhibits a large multiconfigurational character (see Fig. 2). Additionally, the $2\ ^1B_2$ excited state, computed at 5.20 eV with a significant oscillator strength of 0.078, must be also contributing to the experimental band at 5.41 eV.

The following electronic transitions are calculated to have small oscillator strengths. The first rydberg transition,

$1\ ^1A_1 \rightarrow 1\ ^1A_2$, is computed to be at 5.64 eV. It is dipole forbidden and the corresponding wave function implies the single excitation from the HOMO to the first rydberg orbital 3s.

In the high energy region, the experimental spectrum shows an intense band at 6.23 eV.[19] CASPT2 calculations find in this region two excited states, $5\ ^1A_1$ and $6\ ^1A_1$, with remarkably high oscillator strengths (0.263 and 0.379, respectively) separated by only 0.13 eV. These states, lying at 6.09 and 6.22 eV above the ground state, correspond to $\pi \rightarrow \pi^*$ transitions with a strong multiconfigurational character (see Fig. 2). The main contributors to the wave function are the excitations from the HOMO–2 to the LUMO+1 and from the HOMO to the LUMO+2. The small energy spacing between the two transitions and the fact that the same configurations are involved in the two states lead us to conclude that both transitions are probably responsible for the absorption band observed at 6.23 eV. The theoretical description reported here gives new insight into the interpretation of the high energy region of the spectrum, which had been previously studied by means of the Zerner's intermediate neglect of differential overlap (ZINDO) procedure.[19] Such semiempirical calculations were rather limited, underestimating the experimental values by around 0.60–0.70 eV. In this sense, it is worth emphasizing that this region is particularly difficult to describe because of the occurrence of transitions to 3p rydberg states.

In order to check the influence of the geometry on the calculated excitation energies, the excited states of TP were recomputed using the structures optimized both at the B3LYP/cc-pVDZ and CCSD/cc-pVTZ levels. The structural modifications do not yield significant differences on the computed excitation energies. When using the CCSD/cc-pVTZ-optimized geometry, the $1\ ^1B_1$ and $1\ ^1B_2$ states are calculated at 3.20 eV (f=0.009) and 3.42 eV (f=0.030, respectively), thus corroborating the lower energy and smaller intensity of the $n \rightarrow \pi^*$ transition. The $^1A_1$ states determining the most intense transitions are calculated at 3.86 ($2\ ^1A_1$), 5.10 ($3\ ^1A_1$), 6.19 ($5\ ^1A_1$), and 6.22 eV ($6\ ^1A_1$), the nearly degeneration predicted for the $5\ ^1A_1$ and $6\ ^1A_1$ states being in better accord with the experimental band observed at 6.23 eV. The ordering of the electronic states is the same and the maximum deviation between the calculated excitation energies is of 0.1 eV. This validates the use of B3LYP-optimized geometries for CASPT2 calculations.

Time-dependent DFT (TDDFT) calculations were performed at the B3LYP/cc-pVTZ level in order to investigate the performance of this approach to describe the excited states of TP. B3LYP calculations predict the $1\ ^1B_1$ ($n\pi^*$) and $1\ ^1B_2$ ($\pi\pi^*$) states as the lowest-energy states at 3.23 (f=0.002) and 3.39 eV (f=0.029) above the ground state in very good correlation with CASPT2 results (see Table II). However, the third excited state ($2\ ^1A_1$) is calculated at 4.40 eV overestimating by 0.6 eV the CASPT2 excitation energy (3.82 eV). Higher-energy $^1A_1$ excited states, which are responsible of the absorptions observed at 5.41 and 6.23 eV, are not adequately described by TDDFT-B3LYP calculations. These states have a large multiconfigurational character that involves significant contributions from bielectronic excitations, and appear close in energy to the first rydberg states (see Fig. 2 and Table II). B3LYP calculations therefore provide a correct description of the lowest-energy excited states of TP, but they are not accurate enough to account for the excited-states in the high-energy region.

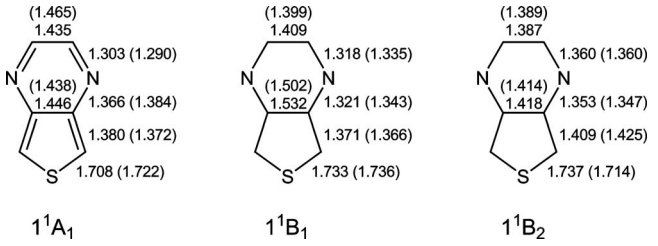

FIG. 4. B3LYP/cc-pVTZ-optimized bond lengths (in angstroms) for the $1\ ^1A_1$ ground state and the $1\ ^1B_1$ and $1\ ^1B_2$ excited states of TP. CASSCF-optimized bond lengths are given within parentheses.

C. Emission spectrum

To shed light on the photophysics of TP, the emission spectrum of TP was computed at the CASPT2 level. As mentioned above, the lowest excited states $1\ ^1B_1$ and $1\ ^1B_2$ are very close in energy and, therefore, both states were considered in the CASSCF/CASPT2 calculations. Figure 4 displays the optimized geometries of the $1\ ^1B_1$ and $1\ ^1B_2$ states, calculated at the TDDFT (B3LYP/cc-pVTZ) level using the TURBOMOLE program,[41] together with that of the $1\ ^1A_1$ ground state. Excitation to both the $1\ ^1B_1$ and the $1\ ^1B_2$ states implies drastic changes with respect to the geometry of the ground state. For the $1\ ^1B_1$ excited state, a lengthening of 0.09 Å is predicted for the C_3-C_4 bond whereas the C–N distances tend to become equal (~1.320 Å). For the $1\ ^1B_2$ excited state, the single/double BLA pattern of the C–C and N–C bonds defining the peripheral 3,6-diaza-octatetraene unit is reversed compared to the ground state. The C_5-C_6, N_1-C_3, and N_2-C_4 bonds have shortened, while the N_1-C_5 and N_2-C_6 bonds have lengthened. The geometrical changes can be rationalized in terms of the bonding and antibonding patterns of the HOMO−1→LUMO ($n \rightarrow \pi^*$) and HOMO →LUMO ($\pi \rightarrow \pi^*$) excitations associated to the $1\ ^1B_1$ and $1\ ^1B_2$ states, respectively. In both excited states, an aromatization of the pyrazine unit can be observed.

The geometries of the ground state and of the $1\ ^1B_1$ and $1\ ^1B_2$ excited states were also optimized at the CASSCF level assuming C_{2v} symmetry and using the ANO basis set employed for CASSCF/CASPT2 calculations. The CASSCF geometries (Fig. 4) support the geometrical changes predicted at the TDDFT level for the $1\ ^1B_1$ and $1\ ^1B_2$ states and confirm the aromatization of the pyrazine unit. The average deviation between TDDFT and CASSCF bond lengths is of 0.015 and 0.009 Å for the $1\ ^1B_1$ and $1\ ^1B_2$ states, respectively. CASSCF calculations therefore support the validity of the geometries provided by the TDDFT approach for the lowest-energy excited states.

Rasmussen *et al.*[19] recorded the emission spectrum of nonsubstituted TP in CH_3CN at room temperature. They observed a fluorescence band with the maximum located at 2.63 eV and a shoulder at 2.86 eV, and attributed it to the relaxation from the first $^1\pi\pi^*$, B_2 state.

The CASSCF/CASPT2 adiabatic transition energies calculated for the $1\ ^1B_1$ and $1\ ^1B_2$ excited states using the DFT-optimized geometries are 2.78 and 2.83 eV, respectively. Almost identical values (2.76 and 2.80 eV, respectively) are obtained when using the geometries optimized at the CASSCF level. These results, obtained in gas phase, reveal that both states are almost degenerate. Consequently, with the aim of answering the question regarding the state responsible for the emission, the effect of the solvent should be also taken into account. As it is well known, the solvent effect on the spectra depends on the nature of the transition. Whereas the $n \rightarrow \pi^*$ transitions generally shift to shorter wavelengths when the polarity of the solvent increases, the $\pi \rightarrow \pi^*$ transitions usually diminish in energy. Our results, calculated in heptane and CH_3CN using the DFT-optimized geometries, support this trend. The energy of the $n\pi^*\ 1\ ^1B_1$ state slightly increases in CH_3CN (2.80 eV), while the $\pi\pi^*\ 1\ ^1B_2$ state is significantly stabilized in going from gas phase to heptane (2.79 eV) and especially to CH_3CN solution (2.52 eV). The shift to lower energies found for the latter can be explained in terms of the electric dipole moment, whose calculated value is multiplied by a factor of 8.1 in passing from the ground state (0.50 D) to the $1\ ^1B_2$ state (4.06 D). A larger solvent effect has to be then expected for the $1\ ^1B_2$ state thus diminishing the emission energy from this state. The bathochromic shift calculated for the $1\ ^1B_2$ state in passing from heptane to CH_3CN (0.27 eV) is in good agreement with the redshift of 0.31 eV experimentally recorded for the emission band of 2,3-dimethyl-TP (λ_{max}, hexane=419 nm, CH_3CN =468 nm).[19] Therefore, CASPT2 calculations predict that the $\pi\pi^*\ 1\ ^1B_2$ state becomes more stable than the $n\pi^*\ 1\ ^1B_1$ state as the polarity of the solvent increases giving support to the idea previously proposed by Rasmussen *et al.*[19] that emission takes place from a $\pi\pi^*$ state.

IV. CONCLUSIONS

In the present contribution, a full interpretation of the absorption spectrum of TP has been provided on the basis of CASSCF/CASPT2 calculations. The $1\ ^1B_1$ ($n\pi^*$) and $1\ ^1B_2$ ($\pi\pi^*$) states are responsible for the low-intensity feature observed at 3.54 eV, the $1\ ^1B_1$ state being predicted to be the lowest-energy excited state. The band observed around 4 eV is assigned to the $2\ ^1A_1$ state, whereas the intense band at 5.41 eV is attributed to a transition to the $3\ ^1A_1$ ($\pi\pi^*$) excited state. Additionally, theoretical calculations give new insight into the interpretation of the high-energy region of the spectrum. The band detected at 6.23 eV is assigned to two different electronic excitations: $1\ ^1A_1 \rightarrow 5\ ^1A_1$ and $1\ ^1A_1 \rightarrow 6\ ^1A_1$. CASSCF/CASPT2 calculations therefore provide an accurate assignment of the experimental absorption bands whenever rydberg and valence states are described separately.

The study of the geometry has revealed that DFT turns out to be a valid alternative to CC methods to establish the molecular structure for this type of systems, which could be important for the study of low-bandgap oligomers and polymers. TDDFT calculations furthermore provide a proper description of the lowest-energy excited states.

Concerning the emission spectrum, CASPT2 results predict that the $1\ ^1B_1$ and $1\ ^1B_2$ states are almost degenerate in gas phase and both states could be responsible of the emission. To disentangle this point, new experiments investigating the polarization of the emission band would be desirable. In solution, the $1\ ^1B_2$ state is calculated to become more stable and the fluorescence observed is assigned to an emission from the $\pi\pi^*$ state.

ACKNOWLEDGMENTS

Financial support by the Ministerio de Ciencia e Innovación (MICINN) of Spain (Project Nos. CTQ2006-14987-C02-02, CTQ2009-08790, and Consolider-Ingenio CSD2007-00010), the Generalitat Valenciana (Grant No. ACOMP/2009/269), and European FEDER funds is acknowledged. The authors thank Professor Luis Serrano-Andrés, Dr. J. J. Serrano-Pérez, and Dr. B. Milián-Medina for fruitful discussions. M.D.G.J. gratefully acknowledges the MICINN for a FPU fellowship.

[1] J. Roncali, Chem. Rev. **97**, 173 (1997); S. C. Rasmussen and M. Pomerantz, in *Handbook of Conducting Polymers*, 3rd ed., edited by T. A. Skotheim and J. R. Reynolds (CRC, Boca Raton, 2007) Vol. 1, Chap. 12; S. C. Rasmussen, K. Ogawa, and S. D. Rothstein, in *Handbook of Organic Electronics and Photonics*, edited by H. S. Nalwa (American Scientific Publishers, Stevenson Ranch, 2007), Vol. 1, Chap. 1.
[2] F. Wudl, M. Kobayashi, and A. J. Heeger, J. Org. Chem. **49**, 3382 (1984).
[3] M. Huskić, D. Vanderzande, and J. Gelan, Synth. Met. **99**, 143 (1999).
[4] P. M. Viruela, R. Viruela, E. Ortí, and J.-L. Brédas, J. Am. Chem. Soc. **119**, 1360 (1997).
[5] K. Nayak and D. S. Marynick, Macromolecules **23**, 2237 (1990).
[6] P. Otto and J. Ladik, Synth. Met. **36**, 327 (1990).
[7] M. Pomerantz, B. Chaloner-Gill, L. O. Harding, J. J. Tseng, and W. J. Pomerantz, J. Chem. Soc., Chem. Commun. **1992**, 1672; Synth. Met. **55**, 960 (1993).
[8] D. D. Kenning and S. C. Rasmussen, Macromolecules **36**, 6298 (2003).
[9] C. Kitamura, S. Tanaka, and Y. Yamashita, J. Chem. Soc., Chem. Commun. **1994**, 1585; S. Tanaka and Y. Yamashita, Synth. Met. **69**, 599 (1995); C. Kitamura, S. Tanaka, and Y. Yamashita, Chem. Mater. **8**, 570 (1996); S. Akoudad and J. Roncali, Chem. Commun. (Cambridge) **1998**, 2081; A. Berlin, G. Zotti, S. Zecchin, G. Schiavon, B. Vercelli, and A. Zanelli, Chem. Mater. **16**, 3667 (2004); I. F. Perepichka, E. Levillain, and J. Roncali, J. Mater. Chem. **14**, 1679 (2004); J. Casado, R. P. Ortiz, M. C. R. Delgado, V. Hernández, J. T. L. Navarrete, J.-M. Raimundo, P. Blanchard, M. Allain, and J. Roncali, J. Phys. Chem. B **109**, 16616 (2005); M. Shahid, R. S. Ashraf, E. Klemm, and S. Sensfuss, Macromolecules **39**, 7844 (2006).
[10] K. R. J. Thomas, J. T. Lin, Y. T. Tao, and C. H. Chuen, Adv. Mater. **14**, 822 (2002); G. Sonmez, C. K. F. Shen, Y. Rubin, and F. Wudl, Angew. Chem., Int. Ed. **43**, 1498 (2004); G. Sonmez, H. B. Sonmez, C. K. F. Shen, and F. Wudl, Adv. Mater. **16**, 1905 (2004); G. Sonmez, H. B. Sonmez, C. K. F. Shen, R. W. Jost, Y. Rubin, and F. Wudl, Macromolecules **38**, 669 (2005); G. Sonmez and F. Wudl, J. Mater. Chem. **15**, 20 (2005); G. Sonmez, C. K. F. Shen, Y. Rubin, and F. Wudl, Adv. Mater. **17**, 897 (2005); W. C. Wu, W. Y. Lee, and W. C. Chen, Macromol. Chem. Phys. **207**, 1131 (2006); W. C. Wu, C. L. Liu, and W. C. Chen, Polymer **47**, 527 (2006).
[11] R. D. Champion, K. F. Cheng, C. L. Pai, W. C. Chen, and S. A. Jenekhe, Macromol. Rapid Commun. **26**, 1835 (2005).
[12] E. Perzon, X. J. Wang, F. L. Zhang, W. Mammo, J. L. Delgado, P. de la Cruz, O. Inganäs, F. Langa, and M. R. Andersson, Synth. Met. **154**, 53 (2005); R. S. Ashraf, M. Shahid, E. Klemm, M. Al-Ibrahim, and S. Sensfuss, Macromol. Rapid Commun. **27**, 1454 (2006); Y. J. Xia, J. Luo, X. Y. Deng, X. Z. Li, D. Y. Li, X. H. Zhu, W. Yang, and Y. Cao, Macromol. Chem. Phys. **207**, 511 (2006); E. Bundgaard and F. C. Krebs, Sol. Energy Mater. Sol. Cells **91**, 954 (2007); W. Mammo, S. Admassie, A. Gadisa, F. L. Zhang, O. Inganäs, and M. T. Andersson, *ibid.* **91**, 1010 (2007).

[13] L. M. Campos, A. Tontcheva, S. Gunes, G. Sonmez, H. Neugebauer, N. S. Sariciftci, and F. Wudl, Chem. Mater. **17**, 4031 (2005); F. L. Zhang, E. Perzon, X. J. Wang, W. Mammo, M. R. Andersson, and O. Inganäs, Adv. Funct. Mater. **15**, 745 (2005); M. M. Wienk, M. G. R. Turbiez, M. P. Struijk, M. Fonrodona, and R. A. J. Janssen, Appl. Phys. Lett. **88**, 153511 (2006); F. L. Zhang, W. Mammo, L. M. Andersson, S. Admassie, M. R. Andersson, and O. Inganäs, Adv. Mater. **18**, 2169 (2006); M. H. Petersen, O. Hagemann, K. T. Nielsen, M. Jorgensen, and F. C. Krebs, Sol. Energy Mater. Sol. Cells **91**, 996 (2007); R. Kroon, M. Lenes, J. C. Hummelen, P. W. M. Blom, and B. D. Boer, Polym. Rev. **48**, 531 (2008).
[14] G. Sonmez and H. B. Sonmez, J. Mater. Chem. **16**, 2473 (2006).
[15] R. Motoyama, D. Sato, and E. Imoto, Nippon Kagaku Zasshi **78**, 793 (1957) [Chem. Abstr. **54**, 22560e (1960)].
[16] D. Binder, C. R. Noe, F. Geissler, and F. Hillebrand, Arch. Pharm. **314**, 564 (1981).
[17] D. D. Kenning, K. A. Mitchell, T. R. Calhoun, M. R. Funfar, D. J. Sattler, and S. C. Rasmussen, J. Org. Chem. **67**, 9073 (2002).
[18] D. J. Sattler, K. A. Mitchell, and S. C. Rasmussen, Abstr. Pap. - Am. Chem. Soc. **225**, U391 (2003).
[19] S. C. Rasmussen, D. J. Sattler, K. A. Mitchell, and J. Maxwell, J. Lumin. **109**, 111 (2004).
[20] G. D. Purvis and R. J. Bartlett, J. Chem. Phys. **76**, 1910 (1982).
[21] A. D. Becke, J. Chem. Phys. **98**, 5648 (1993).
[22] C. Lee, W. Yang, and R. G. Parr, Phys. Rev. B **37**, 785 (1988).
[23] T. H. Dunning, Jr., J. Chem. Phys. **90**, 1007 (1989); R. A. Kendall, T. H. Dunning, and R. J. Harrison, *ibid.* **96**, 6796 (1992); K. A. Peterson, D. E. Wood, and T. H. Dunning, *ibid.* **100**, 7410 (1994).
[24] K. Andersson, P.-Å. Malmqvist, B. O. Roos, A. J. Sadlej, and K. Wolinski, J. Phys. Chem. **94**, 5483 (1990).
[25] K. Andersson, P.-Å. Malmqvist, and B. O. Roos, J. Chem. Phys. **96**, 1218 (1992).
[26] B. O. Roos, K. Andersson, M. P. Fülscher, P.-Å. Malmqvist, L. Serrano-Andrés, K. Pierloot, and M. Merchán, Adv. Chem. Phys. **93**, 219 (1996).
[27] P. O. Widmark, P.-Å. Malmqvist, and B. O. Roos, Theor. Chim. Acta **77**, 291 (1990).
[28] B. O. Roos, M. P. Fülscher, P.-Å. Malmqvist, M. Merchán, and L. Serrano-Andrés, in *Quantum Mechanical Electronic Structure Calculations with Chemical Accuracy*, edited by S. R. Langhoff (Kluwer, Dordrecht, 1995), p. 357.
[29] B. O. Roos and K. Anderson, Chem. Phys. Lett. **245**, 215 (1995); B. O. Roos, K. Andersson, M. P. Fülscher, L. Serrano-Andrés, K. Pierloot, M. Merchán, and V. Molina, J. Mol. Struct.:THEOCHEM **388**, 257 (1996); N. Forsberg and P.-Å. Malmqvist, Chem. Phys. Lett. **274**, 196 (1997).
[30] P.-Å. Malmqvist, Int. J. Quantum Chem. **30**, 479 (1986).
[31] P.-Å. Malmqvist and B. O. Roos, Chem. Phys. Lett. **155**, 189 (1989).
[32] J. Tomasi and M. Persico, Chem. Rev. **94**, 2027 (1994); C. S. Cramer and D. G. Truhlar, in *Solvent Effects and Chemical Reactivity*, edited by O. Tapia and J. Bertrán (Kluwer, Dordrecht, 1996), p. 1.
[33] S. Miertuš, E. Scrocco, and J. Tomasi, Chem. Phys. **55**, 117 (1981); S. Miertus and J. Tomasi, *ibid.* **65**, 239 (1982); M. Cossi, V. Barone, R. Cammi, and J. Tomasi, Chem. Phys. Lett. **255**, 327 (1996); E. Cancès, B. Mennucci, and J. Tomasi, J. Chem. Phys. **107**, 3032 (1997); V. Barone, M. Cossi, and J. Tomasi, J. Comput. Chem. **19**, 404 (1998); M. Cossi, G. Scalmani, N. Rega, and V. Barone, J. Chem. Phys. **117**, 43 (2002).
[34] M. J. Frisch, G. W. Trucks, H. B. Schlegel *et al.*, GAUSSIAN03, (Revision C02), Gaussian, Inc., Wallingford CT, 2004.
[35] G. Karlström, R. Lindh, P.-Å. Malmqvist, B. O. Roos, U. Ryde, V. Veryazov, P.-O. Widmark, M. Cossi, B. Schimmelpfennig, P. Neogrady, and L. Seijo, Comput. Mater. Sci. **28**, 222 (2003).
[36] L. Wen, B. C. Duck, P. C. Dastoor, and S. C. Rasmussen, Macromolecules **41**, 4576 (2008).
[37] L. Wen, J. P. Nietfeld, C. M. Amb, and S. C. Rasmussen, J. Org. Chem. **73**, 8529 (2008).
[38] B. Bak, D. Christensen, L. Hansen-Nygaard, and J. Rastrup-Andersen, J. Mol. Spectrosc. **7**, 58 (1961).
[39] S. W. Schneller, F. W. Clough, and P. N. Skancke, J. Heterocycl. Chem. **13**, 581 (1976).
[40] J. Armand, C. Bellec, L. Boulares, P. Chaquin, D. Masure, and J. Pinson, J. Org. Chem. **56**, 4840 (1991).
[41] The 1 $^1B_1$ and 1 $^1B_2$ excited states were optimized at the TDDFT B3LYP/cc-pVTZ level using the TURBOMOLE program. For both states, TD-DFT calculations led to planar C_{2v} geometries (Fig. 4), which were characterized as true minima with no imaginary frequency. (TURBOMOLE 5.10: Electronic Structure Calculations on Workstation Computers: R. Ahlrichs, M. Bär, M. Häser, H. Horn, and C. Kölmel, Chem. Phys. Lett. **162**, 165 (1989).